Sensors & Actuators: B. Chemical 281 (2019) 746–750

Contents lists available at ScienceDirect

Sensors and Actuators B: Chemical

journal homepage: www.elsevier.com/locate/snb

Highly sensitive electrochemical analysis of tunnel structured MnO_2 nanoparticle-based sensors on the oxidation of nitrite

Yifan Dai[a,b,1], Jianzhi Huang[c,1], Huichun Zhang[c], Chung Chiun Liu[a,b,*]

[a] Department of Chemical and Biomolecular Engineering, Case Western Reserve University, 10900 Euclid Avenue, Cleveland, OH, 44106, USA
[b] Electronics Design Center, Case Western Reserve University, 10900 Euclid Avenue, Cleveland, OH, 44106, USA
[c] Department of Civil Engineering, Case Western Reserve University, 10900 Euclid Avenue, Cleveland, OH, 44106, USA

ARTICLE INFO

Keywords:
Alpha-MnO_2
Nitrite sensing
Micro-plotter
Tunnel structured MnO_2

ABSTRACT

Three MnO_2 nanoparticles with different tunnel structures, α-, β-, and γ-MnO_2, were synthesized and characterized. We demonstrated and compared their capabilities on the electrochemical oxidation of nitrite, providing a new perspective for MnO_2 or MnO_2 based materials on sensing application. α-MnO_2 exhibited higher electrochemical reactivity than β- or γ-MnO_2, which was ascribed to its higher conductivity, more exposure to MnO_6 edges, longer average Mn−O bond length, and lower Mn average oxidation state(AOS). We hereby reported the first α-MnO_2 nanoparticle-based electrochemical sensor for nitrite sensing. A highly controlled micro-plotter was used to deposit the MnO_2 nanoparticles for the sensor fabrication, providing a micro-pattern of the sensing surface area of MnO_2 and ensuring the reproducibility and sensitivity of this MnO_2 based sensor. Using differential pulse voltammetry, a detection range of 10–800 μM of nitrite was accomplished along with a sensitivity of 17.1 μA μM^{-1} and a detection limit of 0.5 μM.

1. Introduction

Nitrite (NO_2^-) is a symmetric anion, which is considered an inorganic pollutant present in food, physiological systems, and the environment [1]. The US Environmental Protection Agency (EPA) established the maximum level of nitrite in drinking water to be 1 mg/L. Nitrite may cause anoxia in fish and other aquatic living species, producing adverse reproductive effects on animals [2,3]. Nitrite is also known to react with nitrosatable compounds in human stomach forming carcinogenic nitrosamines by interaction with amines, which can cause methaemoglorbinaemia by oxidizing hemoglobin to methemoglobin [4]. Many analytical techniques have been developed for nitrite measurement, including Griess method [5], high performance liquid chromatography (HPLC) with UV/vis detector [6], chemiluminescence [7], gas chromatography-mass spectrometry (GC–MS) [8], and capillary electrophoresis [9]. However, these analytical techniques are usually time-consuming, expensive, involving toxic reagents, or requiring skilled operators. Hence, the development of a cost-effective, simple, rapid and sensitive method for the determination of nitrite concentrations is desirable. We hereby demonstrate a simply fabricated, highly sensitive electrochemical sensor for the detection of nitrite using α-MnO_2 nanoparticles.

Compared with noble metals such as palladium and platinum, MnO_2 is thought to be one of the most attractive oxide materials due to its high abundance, low cost, low toxicity, and environmental friendliness [10–13]. In addition, MnO_2 has excellent electro-catalytic properties and high specific capacitance, which have been applied in super-capacitors and developing catalysts for oxygen evolution reactions [14,15]. MnO_2-based material was functioned as an efficient sensing interface for detection of H_2O_2 [16], glucose [17], formaldehyde, [18] and ascorbic acid [19] based on their oxidation behaviors at different electrochemical potentials. One type of electrochemical nitrite sensors also used MnO_2 or MnO_2-based materials [20–22]. However, the phase structure effect of the MnO_2 on these applications is still lacking. The basic unit [MnO_6] links in different ways, therefore MnO_2 exists in different structures, namely, tunnel structure (e.g., α-, β-, and γ-MnO_2) and layer structure (δ-MnO_2). MnO_2 exhibits various oxidative and catalytic reactivity due to differences in their crystal lattice structures, crystal cell parameters, and other surface and structural properties [23,24]. For instance, α-MnO_2 was reported to be more reactive than β- and γ-MnO_2 in catalytic oxidation of phenol, owing to its high surface area, oxygen loss, as well as double tunneled structure [25]. In addition,

* Corresponding author at: Department of Chemical and Biomolecular Engineering, Case Western Reserve University, 10900 Euclid Avenue, Cleveland, OH, 44106, USA.
E-mail address: cxl9@case.edu (C.C. Liu).
[1] Authors contribute equally.

https://doi.org/10.1016/j.snb.2018.11.014
Received 10 July 2018; Received in revised form 15 October 2018; Accepted 4 November 2018
Available online 05 November 2018
0925-4005/

CO oxidation by different structured MnO_2 follows the order: α- ≈ δ- > γ- > β-MnO_2, due to the difference in the crystal phase and channel structures of the MnO_2 [26]. Previous studies regarding electrochemical nitrite sensors using MnO_2 or MnO_2 based materials focused only on one structure. For instance, uniform β-MnO_2 was synthesized for electrochemical oxidation of nitrite [20]. Hence, specifically, there was a lack of understanding on the effect of phase structure of MnO_2 on fabrication of high-sensitivity sensing devices. Furthermore, the effect of phase structures of MnO_2 on oxidative and catalytic reactivity of MnO_2 *per se* was not clearly understood. Therefore, the assessment of different phase structured MnO_2 on electrochemical oxidation behavior is critical for developing high-sensitivity sensing platform using MnO_2 or MnO_2-based materials.

For sensing device fabrication, we used a well-characterized, cost-effective three-electrode sensor platform with gold thin films as the working and counter electrode and a thick film printed Ag/AgCl as the reference electrode. The fabrication and configuration of the sensors and their reproducibility and stability were described and characterized in previous studies [27,28]. For nanoparticle-based sensor fabrication, an inkjet-printer was typically used for non-direct printing of nanoparticles on electronics [29–31]. We hereby demonstratea direct printing method using piezoelectric based micro-plotter for nanoparticle deposition. Compared with conventional inkjet-printers, the micro-plotter directly "writes" (with contact) on the surface of the substrate, providing a well-defined nanoparticle pattern. Moreover, the application of piezoelectric on the "writing" tip ensured the weight of the deposited nanoparticles which was identical from batch to batch based on the constant AC current applied [32–34], delivering a highly reproducible materialization of the nanoparticle surface.

2. Experiments and materials

(Shown in the SI).

3. Results and discussion

We first synthesized three different phase structures of MnO_2 using simple one-step synthesis methods (details in the SI). X-ray diffraction (XRD) and scanning electron microscopy (SEM) were employed for material characterization. In Fig. 1a, the phase structures of the three synthesized MnO_2 were confirmed by the XRD patterns, where the peak positions of each MnO_2 sample were precisely matched to the corresponding standard patterns in the inorganic crystallographic database or previous reports [23,24]. SEM images were obtained to assess the morphologies of the different MnO_2 (Fig. 1b). Though α-MnO_2 in the SEM images appeared to have layered structures, it was nanofiber as shown in the high resolution transmission electron microscopy (HRTEM) images with a diameter of 5 ~ 20 nm and the length of 60 ~ 120 nm (Fig. S1). For β-MnO_2, the diameter was 5–100 nm and the length was 0.4–1.4 μm. γ-MnO_2 was also nanofiber with a diameter of 10–30 nm and the length was around 1–2 μm. The nanofiber would accumulate together forming a sphere with a diameter 4 μm.

Cyclic voltammetry (CV) was applied as the signal transduction mechanism for the determination of the oxidative reactivity of different phases of MnO_2 toward 5 mM nitrite ions in order to compare the sensitivity of MnO_2 based sensors. The reactivity of α-MnO_2, β-MnO_2 or γ-MnO_2 particles was examined individually. Each type of MnO_2 ink was prepared with the same concentration of 10 mg mL^{-1} and directly applied to the micro-plotter for sensors fabrication based on the gold sensor prototype (the ink preparation and sensor printing procedures are shown in Text S5 and Fig S2, respectively). The microscope graphs of the MnO_2 sensors before and after printing are shown in Fig. 1c. 5 mM of sodium nitrite solution in 0.1 M PBS solution was used as the analyte for sensor sensitivity comparison. The oxidation potential was identified at +0.65 V using CV scans over the voltage range of +0 to +1.2 V, as shown in Fig. 2a (the parameters and procedures for the CV measurement are shown in Text S5). The gold sensor prototype was also used for electrochemical oxidation of nitrite in order to compare the sensitivity, as shown in the green line of Fig. 2a. The α-MnO_2-based sensor showed the highest anodic current outputs based on the oxidative catalytic reaction of MnO_2 with nitrite ions compared with that of γ-MnO_2 or β-MnO_2. Therefore, α-MnO_2 was selected as the sensor substrate material for further investigation of the sensitivity and selectivity of nitrite detection in different environment conditions. The proposed mechanism for nitrite oxidation might follow reactions based on a previous research [21].

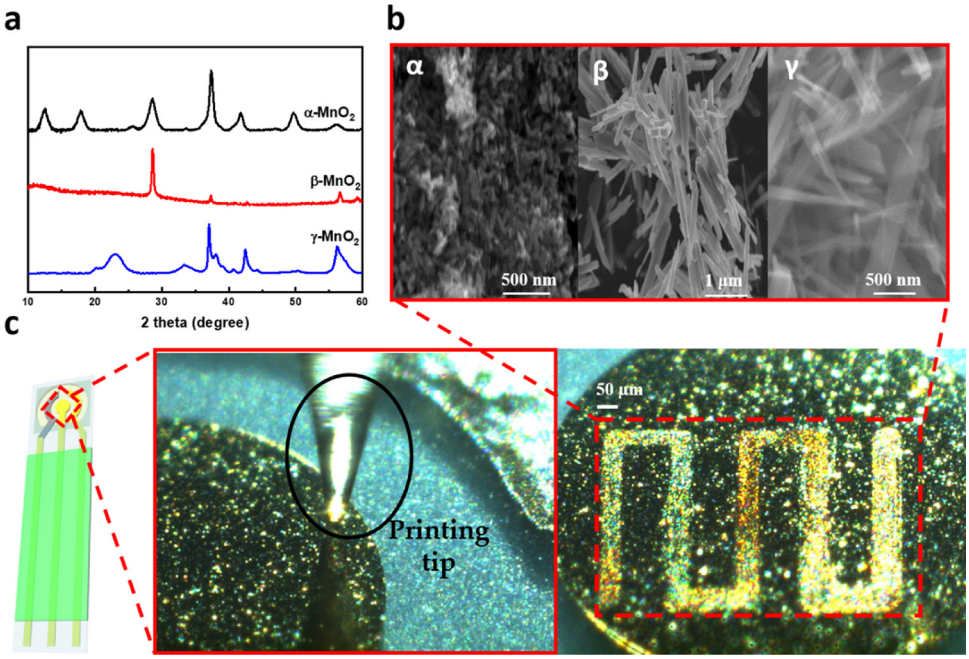

Fig. 1. a. XRD pattern of different tunnel structured MnO_2. b. SEM images of different tunnel structured MnO_2. c. Gold sensor before (left) and after (right) printing of MnO_2 pattern on the working electrode.

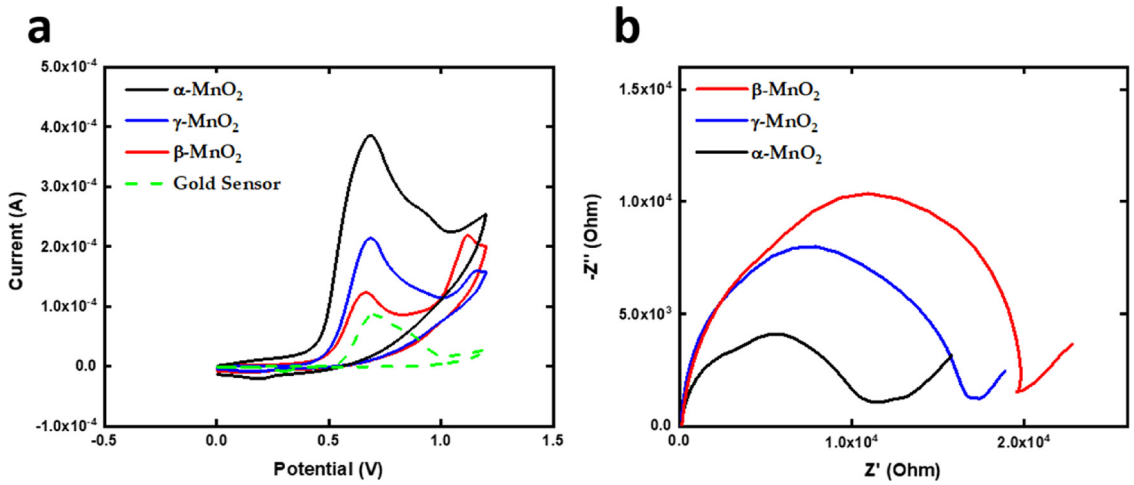

Fig. 2. a. CV scans of different MnO_2 sensors for oxidation of 5 mM nitrite ions in 0.1 M PBS. b. Nyquist plot of different MnO_2 sensors for comparison of their relative surface conductivity.

$$Mn^{4+}O_2 + NO_2^- \leftrightarrow (Mn^{4+}O_2 - NO_2^-)$$

$$(Mn^{4+}O_2 - NO_2^-) \leftrightarrow (Mn^{5+}O_2 - NO_2^-) + e^-$$

$$(Mn^{5+}O_2 - NO_2^-) \leftrightarrow (Mn^{5+}O_2 - NO_2) + e^-$$

$$NO_2 + H_2O \leftrightarrow 2H^+ + NO_2^- + NO_3^-$$

$$NO_2 + H_2O \leftrightarrow 2H^+ + NO_3^- + 2e^-$$

$$(Mn^{5+}O_2 - NO_2) \leftrightarrow Mn^{4+}O_2$$

There are several reasons for α-MnO_2 to show better sensitivity than β- and γ-MnO_2. First, the conductivity of different MnO_2 was examined. Electrochemical impedance spectroscopy (EIS) was used to investigate the interfacial surface conductivity of the different MnO_2 printed sensors using redox coupling $[Fe(CN)_6]^{3-/4-}$ (The EIS procedure is shown in Text S7). $[Fe(CN)_6]^{3-/4-}$ was used to indicate the conductivity on the sensor surface at the amplitude of 0.05 V. As shown in Fig. 2b, the conductivity follows the order: α-MnO_2 > γ-MnO_2 > β-MnO_2, which agrees well with the oxidation sensitivity sequence shown in Fig. 2a.

Moreover, it has been reported that MnO_2 with longer Mn-O bonds would have lower Mn-O bond strength, indicating that MnO_2 can be reduced at lower temperature. Previous studies demonstrated that MnO_2 with longer Mn-O bond length was better oxidative degradation of sulfamethoxazole [35] and catalytic reactivity for water oxidation [36]. As shown in Table 1, similar results were found in electrochemical oxidation of nitrite. The average Mn-O distance of α-, β-, and γ-MnO_2 was reported to be 1.925, 1.888, and 1.91 Å, respectively. These bond lengths illustrated the sensitivity of different structured MnO_2 based sensors with a decreasing order: α-MnO_2 > γ-MnO_2 > β-MnO_2.

Also, it was shown that surface energies would decrease as decreasing average manganese oxidation state, resulting in improving its functionality [38]. For instance, lower Mn AOS improved water oxidation catalysis, owing to its higher content of Mn(III) [39]. The Mn AOS in this study decreased in the following order: α-MnO_2 < γ-MnO_2 < β-MnO_2, which was in agreement with its nitrite sensitivity, indicating that Mn AOS might play an important role in the electrochemical oxidation of nitrite.

Table 1
BET Surface Area, Mn Average Oxidation State (AOS), and average Mn-O bond length.

MnO_2	Surface area (m^2/g) [10]	AOS	Avg. Mn-O, Å
α-MnO_2	175	3.72 ± 0.12	1.925 [37]
β-MnO_2	168	3.84 ± 0.09	1.888 [37]
γ-MnO_2	73	3.79 ± 0.03	1.910 [26]

Another possible reason could be the difference of their structures. For the three tunnel structured MnO_2 investigated, α-MnO_2 contained both edge-sharing and corner-sharing MnO_6, and with a large tunnels size (2 × 2). β-MnO_2 contained corner-shared MnO_6, allowing only the formation of small tunneled size (1 × 1) [40,41]. Similar to α-MnO_2, γ-MnO_2 also contained both edge-sharing and corner-sharing MnO_6 providing two types of tunnel size: one was (1 × 1) tunnels of pyrolusite, and the other was (1 × 2) tunnels of ramsdellite [42]. Therefore, the sensitivity of α- or γ-MnO_2 was better than that of the single-tunnel structured β-MnO_2, which might be due to the more exposure of MnO_6 edges, and was similar to a previous study on their catalytic reactivity [25].

Differential pulse voltammetry (DPV) was applied as a highly-sensitive transduction mechanism for electrochemical measurement [28,43–46]. DPV was used to quantify different concentrations of nitrite ions (the parameters and procedures for DPV measurement are shown in Text S9). As shown in Fig. 3a, the oxidation potential was identical as that in the CV measurement. A concentration range of 800μM to 10μM of nitrite was analyzed by the α-MnO_2-based sensor. A detection limit of 0.5 μM was achieved (light blue line in Fig. 3a). The calibration curve of the DPV measurements is shown in Fig. 3b with a R-square value of 0.967 (n > 3). A high-sensitivity of 17.1 μA μM^{-1} was achieved based on this sensing platform.

In order to confirm the selectivity of this nitrite sensor, common food-containing chemicals, such as glucose, uric acid, and ascorbic acid, which also embrace positive oxidation potentials, were used to conduct the interference study [20]. 3 mM of glucose, 1 mM of uric acid, and 1 mM of ascorbic acid were mixed in 0.1 M PBS solution at pH = 7.4. We first tested the oxidation capability of the interference solution only. As shown in Fig. 3c red line, a small oxidation peak was shown at + 0.3 V, which correlates with the oxidative behavior of the interference chemicals. Different concentrations of nitrite were then prepared in the interference solution and compared with the nitrite solution prepared in 0.1 M PBS. As shown in Fig. 3c, for the same concentration of nitrite, the oxidation peak at around 0.5 V overlapped with each other even though an oxidation peak at + 0.3 V remained, indicating the addition of glucose, uric acid, and ascorbic did not interfere with the detection of nitrite. In general, non-enzymatic metal oxide based sensors could only oxidize glucose, uric acid and ascorbic acid in basic conditions [47]. Therefore, under neutral pH conditions, we observed no interference for the quantification of nitrite.

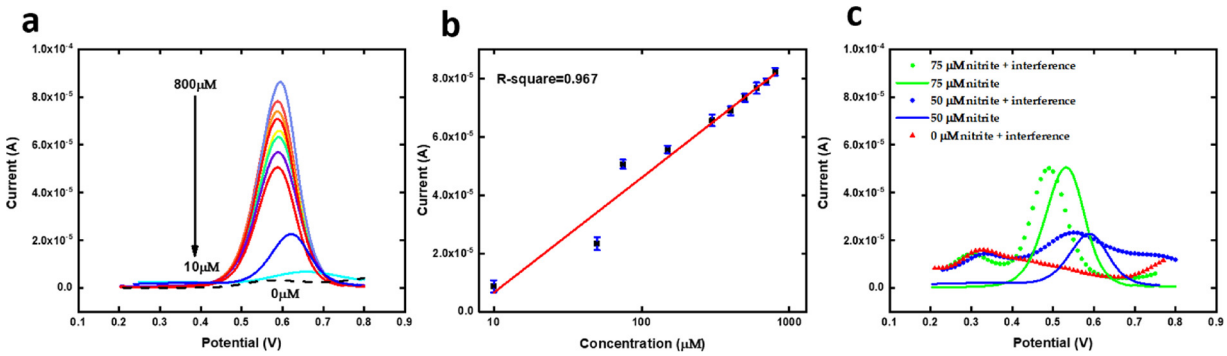

Fig. 3. a) DPV measurements of nitrite in 0.1 M PBS from 800 μM to 10 μM. b) Calibration curve based on DPV current outputs against concentrations (n > 3). c) Interference study based on glucose, uric acid, ascorbic acid in 0.1 M PBS.

4. Conclusion

In summary, a highly-sensitive MnO_2 structure was identified for electrochemical oxidation applications. A precisely-controlled piezoelectric based nanoparticle-printing technique was applied for MnO_2 based sensor fabrication, providing high sensitivity and reproducibility. Differential pulse voltammetry with a detection range of 800 μM to 10 μM was accomplished along with a high sensitivity of 17.1 μA μM^{-1} and a detection limit of 0.5 μM. Our study on the electrochemical oxidation behavior of different structured MnO_2 provided a new perspective for the development of MnO_2 or MnO_2 related materials-based sensing devices.

Conflicts of interests

The authors declare no conflicts of interests.

Authors contributions

CCL, HZ, YD and JH conceived and designed the experiments. YD and JH conducted the experiments. YD, JH, HZ, CCL analyzed data. YD, JH, HZ, CCL prepared this manuscript.

Acknowledgements

Support of this research by Wallace R. Persons research fund of Case Alumni Association is gratefully appreciated and acknowledged. Portion of this research is supported by National Science Foundation under grant number: #CBET-1762691, which is also acknowledged. The usage of the facilities in the Electronics Design Center of CWRU is also greatly appreciated

Appendix A. Supplementary data

Supplementary material related to this article can be found, in the online version, at doi:https://doi.org/10.1016/j.snb.2018.11.014.

References

[1] S. Radhakrishnan, K. Krishnamoorthy, C. Sekar, J. Wilson, S.J. Kim, A highly sensitive electrochemical sensor for nitrite detection based on Fe2O3 nanoparticles decorated reduced graphene oxide nanosheets, Appl. Catal. B 148–149 (2014) 22–28.
[2] A.M. Fan, V.E. Steinberg, Health implications of nitrate and nitrite in drinking water: an update on methemoglobinemia occurrence and reproductive and developmental toxicity, Regul. Toxicol. Pharmacol. 23 (1) (1996) 35–43.
[3] W.M. Lewis Jr, D.P. Morris, Toxicity of nitrite to fish: a review, Trans. Am. Fish. Soc. 115 (2) (1986) 183–195.
[4] A. Boink, G. Speijers, Health effects of nitrates and nitrites, a review, International Conference on Environmental Problems Associated with Nitrogen Fertilisation of Field Grown Vegetable Crops 563 (1999) 29–36.
[5] P. Kleinbongard, T. Rassaf, A. Dejam, S. Kerber, M. Kelm, Griess method for nitrite measurement of aqueous and protein-containing samples, Methods Enzymol. (2002) 158–168 Elsevier.
[6] R.J. Kieber, P.J. Seaton, Determination of subnanomolar concentrations of nitrite in natural waters, Anal. Chem. 67 (18) (1995) 3261–3264.
[7] M.M. Pelletier, P. Kleinbongard, L. Ringwood, R. Hito, C.J. Hunter, A.N. Schechter, M.T. Gladwin, A. Dejam, The measurement of blood and plasma nitrite by chemiluminescence: pitfalls and solutions, Free Radic. Biol. Med. 41 (4) (2006) 541–548.
[8] S.M. Helmke, M.W. Duncan, Measurement of the NO metabolites, nitrite and nitrate, in human biological fluids by GC–MS, J. Chromatogr. B 851 (1–2) (2007) 83–92.
[9] A. Leone, P. Francis, P. Rhodes, S. Moncada, A rapid and simple method for the measurement of nitrite and nitrate in plasma by high performance capillary electrophoresis, Biochem. Biophys. Res. Commun. 200 (2) (1994) 951–957.
[10] J. Huang, S. Zhong, Y. Dai, C.-C. Liu, H. Zhang, Effect of MnO2 phase structure on the oxidative reactivity toward bisphenol a degradation, Environ. Sci. Technol. 52 (19) (2018) 11309–11318.
[11] X. Lu, T. Zhai, X. Zhang, Y. Shen, L. Yuan, B. Hu, L. Gong, J. Chen, Y. Gao, J. Zhou, WO3–x@ Au@ MnO2 core–shell nanowires on carbon fabric for high-performance flexible supercapacitors, Adv. Mater. 24 (7) (2012) 938–944.
[12] A.T. Stone, Reductive dissolution of manganese (III/IV) oxides by substituted phenols, Environ. Sci. Technol. 21 (10) (1987) 979–988.
[13] S. Taujale, L.R. Baratta, J. Huang, H. Zhang, Interactions in ternary mixtures of MnO_2, Al_2O_3, and natural organic matter (NOM) and the impact on MnO_2 oxidative reactivity, Environ. Sci. Technol. 50 (5) (2016) 2345–2353.
[14] M. Toupin, T. Brousse, D. Bélanger, Charge storage mechanism of MnO2 electrode used in aqueous electrochemical capacitor, Chem. Mater. 16 (16) (2004) 3184–3190.
[15] W. Xiao, D. Wang, X.W. Lou, Shape-controlled synthesis of MnO2 nanostructures with enhanced electrocatalytic activity for oxygen reduction, J. Phys. Chem. C 114 (3) (2009) 1694–1700.
[16] L. Li, Z. Du, S. Liu, Q. Hao, Y. Wang, Q. Li, T. Wang, A novel nonenzymatic hydrogen peroxide sensor based on MnO2/graphene oxide nanocomposite, Talanta 82 (5) (2010) 1637–1641.
[17] J. Chen, W.-D. Zhang, J.-S. Ye, Nonenzymatic electrochemical glucose sensor based on MnO2/MWNTs nanocomposite, Electrochem. commun. 10 (9) (2008) 1268–1271.
[18] C. Xie, L. Xiao, M. Hu, Z. Bai, X. Xia, D. Zeng, Fabrication and formaldehyde gas-sensing property of ZnO–MnO2 coplanar gas sensor arrays, Sens. Actuators B: Chem. 145 (1) (2010) 457–463.
[19] X.-L. Luo, J.-J. Xu, W. Zhao, H.-Y. Chen, Ascorbic acid sensor based on ion-sensitive field-effect transistor modified with MnO2 nanoparticles, Anal. Chim. Acta 512 (1) (2004) 57–61.
[20] J.-J. Feng, P.-P. Zhang, A.-J. Wang, Y. Zhang, W.-J. Dong, J.-R. Chen, One-pot hydrothermal synthesis of uniform β-MnO2 nanorods for nitrite sensing, J. Colloid Interface Sci. 359 (1) (2011) 1–8.
[21] N. Jaiswal, I. Tiwari, C.W. Foster, C.E. Banks, Highly sensitive amperometric sensing of nitrite utilizing bulk-modified MnO2 decorated graphene oxide nanocomposite screen-printed electrodes, Electrochim. Acta 227 (2017) 255–266.
[22] C. Xia, W. Ning, G. Lin, Facile synthesis of novel MnO2 hierarchical nanostructures and their application to nitrite sensing, Sens. Actuators B: Chem. 137 (2) (2009) 710–714.
[23] Y. Meng, W. Song, H. Huang, Z. Ren, S.-Y. Chen, S.L. Suib, Structure–property relationship of bifunctional MnO2 nanostructures: highly efficient, ultra-stable electrochemical water oxidation and oxygen reduction reaction catalysts identified in alkaline media, J. Am. Chem. Soc. 136 (32) (2014) 11452–11464.
[24] R. Pokhrel, M.K. Goetz, S.E. Shaner, X. Wu, S.S. Stahl, The “best catalyst” for water oxidation depends on the oxidation method employed: a case study of manganese oxides, J. Am. Chem. Soc. 137 (26) (2015) 8384–8387.
[25] E. Saputra, S. Muhammad, H. Sun, H.M. Ang, M. Tade, S. Wang, Different crystallographic one-dimensional MnO2 nanomaterials and their superior performance in catalytic phenol degradation, Environ. Sci. Technol. 47 (11) (2013) 5882–5887.
[26] S. Liang, F. Teng, G. Bulgan, R. Zong, Y. Zhu, Effect of phase structure of MnO_2 nanorod catalyst on the activity for CO oxidation, J. Phys. Chem. C 112 (14) (2008) 5307–5315.
[27] Y. Dai, A. Molazemhosseini, C.C. Liu, A single-use, in vitro biosensor for the detection of T-tau protein, a biomarker of neuro-degenerative disorders, in PBS and

human serum using differential pulse voltammetry (DPV), Biosensors 7 (1) (2017) 10.
[28] Y. Dai, C. Wang, L.-Y. Chiu, K. Abbasi, B.S. Tolbert, G. Sauvé, Y. Yen, C.-C. Liu, Application of bioconjugation chemistry on biosensor fabrication for detection of TAR-DNA binding protein 43, Biosens. Bioelectron. 117 (2018) 60–67.
[29] G. Hu, T. Albrow-Owen, X. Jin, A. Ali, Y. Hu, R.C. Howe, K. Shehzad, Z. Yang, X. Zhu, R.I. Woodward, Black phosphorus ink formulation for inkjet printing of optoelectronics and photonics, Nat. Commun. 8 (1) (2017) 278.
[30] M. Park, J. Im, M. Shin, Y. Min, J. Park, H. Cho, S. Park, M.-B. Shim, S. Jeon, D.-Y. Chung, Highly stretchable electric circuits from a composite material of silver nanoparticles and elastomeric fibres, Nat. Nanotechnol. 7 (12) (2012) 803.
[31] W. Shen, X. Zhang, Q. Huang, Q. Xu, W. Song, Preparation of solid silver nanoparticles for inkjet printed flexible electronics with high conductivity, Nanoscale 6 (3) (2014) 1622–1628.
[32] A. Marshall, J. Hodgson, DNA chips: an array of possibilities, Nat. Biotechnol. 16 (1) (1998) 27.
[33] J. Ngeh-Ngwainbi, A.A. Suleiman, G.G. Guilbault, Piezoelectric crystal biosensors, Biosens. Bioelectron. 5 (1) (1990) 13–26.
[34] Z.L. Wang, J. Song, Piezoelectric nanogenerators based on zinc oxide nanowire arrays, Science 312 (5771) (2006) 242–246.
[35] J. Wan, L. Zhou, H. Deng, F. Zhan, R. Zhang, Oxidative degradation of sulfamethoxazole by different MnO2 nanocrystals in aqueous solution, J. Mol. Catal. A: Chem. 407 (2015) 67–74.
[36] D.M. Robinson, Y.B. Go, M. Greenblatt, G.C. Dismukes, Water oxidation by λ-MnO2: catalysis by the cubical Mn4O4 subcluster obtained by delithiation of spinel LiMn2O4, J. Am. Chem. Soc. 132 (33) (2010) 11467–11469.
[37] D.M. Robinson, Y.B. Go, M. Mui, G. Gardner, Z. Zhang, D. Mastrogiovanni, E. Garfunkel, J. Li, M. Greenblatt, G.C. Dismukes, Photochemical water oxidation by crystalline polymorphs of manganese oxides: structural requirements for catalysis, J. Am. Chem. Soc. 135 (9) (2013) 3494–3501.
[38] N. Birkner, A. Navrotsky, Thermodynamics of manganese oxides: effects of particle size and hydration on oxidation-reduction equilibria among hausmannite, bixbyite, and pyrolusite, Am. Mineral. 97 (8–9) (2012) 1291–1298.
[39] I.G. McKendry, S.K. Kondaveeti, S.L. Shumlas, D.R. Strongin, M.J. Zdilla, Decoration of the layered manganese oxide birnessite with Mn (II/III) gives a new water oxidation catalyst with fifty-fold turnover number enhancement, Dalton Trans. 44 (29) (2015) 12981–12984.
[40] V.B.R. Boppana, S. Yusuf, G.S. Hutchings, F. Jiao, Nanostructured alkaline-cation-containing δ-MnO2 for photocatalytic water oxidation, Adv. Funct. Mater. 23 (7) (2013) 878–884.
[41] X. Duan, J. Yang, H. Gao, J. Ma, L. Jiao, W. Zheng, Controllable hydrothermal synthesis of manganese dioxide nanostructures: shape evolution, growth mechanism and electrochemical properties, CrystEngComm 14 (12) (2012) 4196–4204.
[42] J. Yuan, K. Laubernds, Q. Zhang, S.L. Suib, Self-assembly of microporous manganese oxide octahedral molecular sieve hexagonal flakes into mesoporous hollow nanospheres, J. Am. Chem. Soc. 125 (17) (2003) 4966–4967.
[43] T. Alizadeh, S. Azizi, Graphene/graphite paste electrode incorporated with molecularly imprinted polymer nanoparticles as a novel sensor for differential pulse voltammetry determination of fluoxetine, Biosens. Bioelectron. 81 (2016) 198–206.
[44] Y. Dai, C.C. Liu, A simple, cost-effective sensor for detecting lead ions in water using under-potential deposited bismuth sub-layer with differential pulse voltammetry (DPV), Sensors 17 (5) (2017) 950.
[45] J. Das, I. Ivanov, L. Montermini, J. Rak, E.H. Sargent, S.O. Kelley, An electrochemical clamp assay for direct, rapid analysis of circulating nucleic acids in serum, Nat. Chem. 7 (7) (2015) 569.
[46] K.M. Koo, L.G. Carrascosa, M.J. Shiddiky, M. Trau, Poly (A) extensions of miRNAs for amplification-free electrochemical detection on screen-printed gold electrodes, Anal. Chem. 88 (4) (2016) 2000–2005.
[47] Y. Dai, A. Molazemhosseini, K. Abbasi, C.C. Liu, A cuprous oxide thin film non-enzymatic glucose sensor using differential pulse voltammetry and other voltammetry methods and a comparison to different thin film electrodes on the detection of glucose in an alkaline solution, Biosensors 8 (1) (2018) 4.